ACS OMEGA

http://pubs.acs.org/journal/acsodf

Article

Separation of Excess Fluoride from Water Using Amorphous and Crystalline AlOOH Adsorbents

Wei-Zhuo Gai,* Shi-Hu Zhang, Yang Yang, Xianghui Zhang, and Zhen-Yan Deng

Cite This: *ACS Omega* 2021, 6, 16488−16497

Read Online

ACCESS | Metrics & More | Article Recommendations

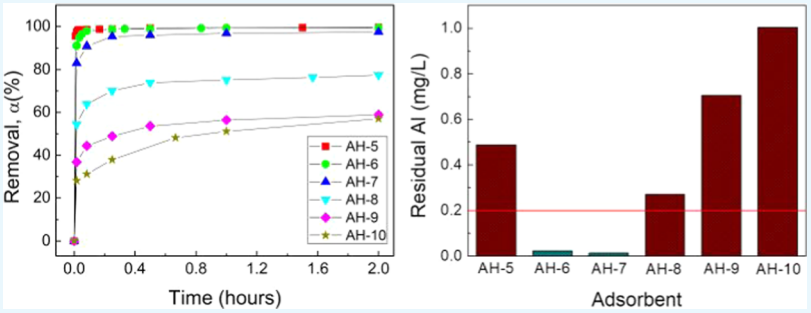

ABSTRACT: Aluminum hydroxide is an effective defluoridation adsorbent; however, the poor defluoridation performance limits its wide application. In this work, amorphous and crystalline AlOOH adsorbents are synthesized through hydrolysis of Al salts, and their defluoridation performances are evaluated in terms of adsorption capacity and rate, sensitivity to pH value, and water quality after defluoridation. The defluoridation performance of AlOOH is closely related to the hydrolysis pH value, but hardly to the type of Al salts. The adsorbent can remove >95% fluoride in the first 2 min and reach adsorption equilibrium within 2 h, and the maximum defluoridation capacity is 41.9 mg/g. Furthermore, the adsorbent exhibits an excellent defluoridation efficiency at a wide pH range of 4.5−10.5. After fluoride removal, the adsorbents prepared at pH values of 6 and 7 exhibit low residual Al concentration. The Fourier transform infrared (FTIR) and X-ray photoelectron spectroscopy (XPS) results confirm that the fluoride removal mechanism is the ligand exchange between fluoride and hydroxyl groups. The excellent defluoridation capacity and low residual Al demonstrate that AlOOH is a potential adsorbent for fluoride separation from water.

1. INTRODUCTION

Fluorine is one of the necessary trace elements for human health and has a significant impact on human bones and teeth. As the human body takes in fluorine mainly through drinking water,[1] the content of fluoride in drinking water is an important parameter of water quality, which determines whether fluoride has beneficial or harmful effects on human health. When the fluoride concentration in drinking water is 0.5−1.5 mg/L, it is helpful to prevent dental caries and maintain the stability of calcium and phosphorus metabolism. However, long-term drinking high fluoride water (>1.5 mg/L) can lead to a series of fluorosis-related diseases, e.g., dental fluorosis, skeletal fluorosis, joint stiffness, paralysis, thyroid dysfunction, and kidney dysfunction.[2] The World Health Organization (WHO) has set 1.5 mg/L as the guideline for fluoride concentration in drinking water.[3] More than 35 countries globally face the problem that the fluoride concentration in drinking water exceeds the WHO guideline, especially in China, India, Pakistan, South Africa, Turkey, Argentina, and Mexico.[4] Therefore, how to reduce the fluoride concentration in drinking water below the WHO guideline is an urgent issue worldwide.

Among various defluoridation technologies, adsorption is an eye-catching, well-studied, and widely used fluoride removal method owing to its simple design, convenient operation, and low cost.[5] Different adsorbents exhibit different defluoridation performances, which depend on the physicochemical properties of adsorbents. During the past decades, a variety of adsorbents have been developed and used for fluoride removal, such as natural-mineral-based adsorbents,[6,7] biomass adsorbents,[8] carbon-based adsorbents,[9−12] metal oxides, or hydroxides.[13−16] For example, stilbite zeolite with low cost was used as the raw material to prepare a nano-hydroxyapatite/stilbite adsorbent, which had an adsorption capacity of 4.02 mg/g.[17] Affonso et al. synthesized an adsorbent by stabilizing carbon nanotubes in chitosan sponge and evaluated its feasibility for

Received: March 26, 2021
Accepted: May 31, 2021
Published: June 14, 2021

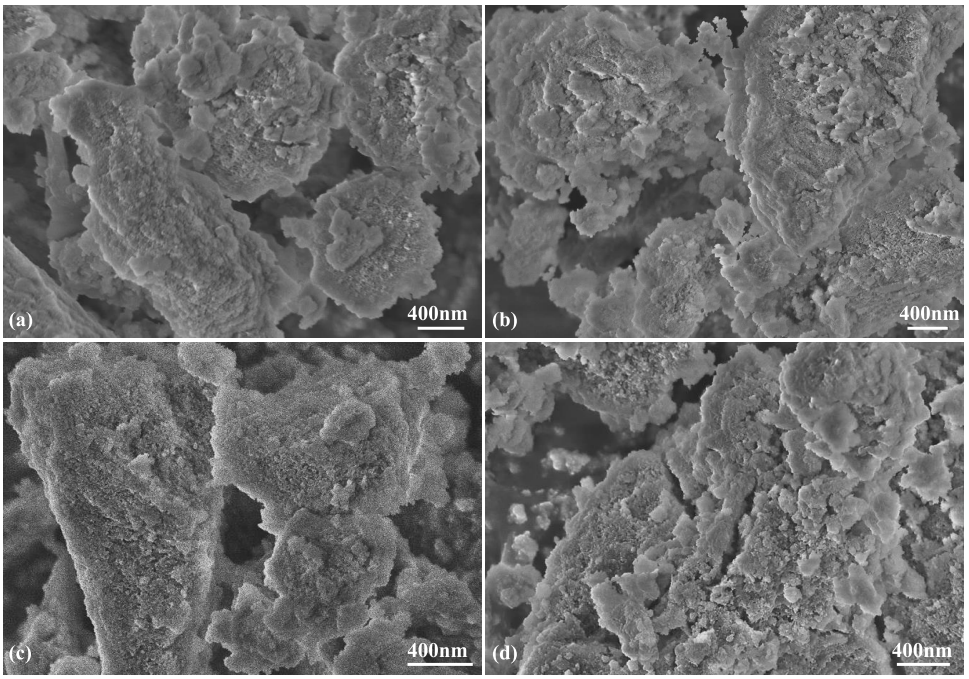

Figure 1. SEM micrographs of (a) AH-5, (b) AH-7, (c) AH-8, and (d) AH-10 adsorbents.

fluoride removal from fertilizer industry wastewater.[18] The adsorbent exhibited excellent renewability, and its adsorption capacity was as high as 975.4 mg/g. Fe−Mg−La trimetal hydroxides prepared through coprecipitation had a maximum defluoridation capacity of 47.2 mg/g.[19] He et al. fabricated a hydroxyapatite nanowire adsorbent using a solvothermal method and found that the fluoride removal mechanisms were electrostatic interactions and anion exchange.[20]

Compared with other adsorbents, Al-based adsorbents have the advantages of simple preparation, low cost, and strong affinity for fluoride, making them extensively researched and used adsorbents for fluoride removal.[1] Although activated alumina is widely used for fluoride removal in vast rural areas, its adsorption capacity is very low (1.45 mg/g).[21,22] Recently, some researchers have found that the defluoridation performance of alumina could be improved by altering the microstructure or the crystalline phase of alumina.[23−26] For example, ordered mesoporous alumina prepared using aluminum isopropoxide as a precursor had a defluoridation capacity of 135 mg/g.[25] Three-dimensional (3D) broccolilike amorphous alumina exhibited an excellent defluoridation capacity of 126.9 mg/g.[26] In addition, surface modification is also an effective method to enhance the defluoridation performance of alumina. The adsorption capacity of mesoporous alumina was increased from 24.45 to 37.35 mg/g by loading MgO on its surface.[27] Surface modification by H_2O_2 can increase the surface hydroxyl groups of alumina, resulting in the enhancement of defluoridation capacity.[28] However, George et al. demonstrated that the residual Al content after defluoridation by alumina was high, which cast a shadow on its wide application.[29]

Besides alumina, aluminum hydroxide is also an effective defluoridation adsorbent, and its residual Al content after defluoridation is much lower than that of alumina. However, the fluoride removal performance of commercial aluminum hydroxide is poor.[1] To enhance the defluoridation efficiency of aluminum hydroxide, some methods were developed.[30−33] Liu et al. investigated the defluoridation performance of freshly prepared aluminum hydroxide.[34] Du et al. researched the effect of aging temperature and additives on the defluoridation capacity of aluminum hydroxide and found that the addition of sulfate greatly enhanced the defluoridation capacity.[35] Jia et al. synthesized a bayerite/boehmite adsorbent with 3D featherlike structures using a hydrothermal method.[36] It is interesting that aluminum hydroxides prepared by different methods possess obvious different defluoridation performances, but there is no literature on this issue. In fact, aluminum hydroxides reported in the literature were prepared using different Al sources under different pH values, which may be the reason for the different defluoridation capacities of aluminum hydroxides prepared by different methods. To clarify this problem, amorphous and crystalline AlOOH adsorbents were synthesized through hydrolysis of Al salts in this work, and the effects of the hydrolysis pH value and the type of Al salts on defluoridation performance were analyzed. Furthermore, the physicochemical mechanisms involved in fluoride removal were revealed.

2. RESULTS AND DISCUSSION

2.1. Characterization of AlOOH Adsorbents. Figure 1 presents the micrographs of AlOOH adsorbents prepared at different hydrolysis pH values. It is found that the morphologies of different AlOOH adsorbents have no obvious difference. Unlike the smooth surface of commercial AlOOH,[37] the surfaces of AlOOH adsorbents are much rougher, making them have large surface areas. There are numerous agglomerates in AlOOH adsorbents, and the size of agglomerates ranges from submicrons to microns.

Figure 2 shows the X-ray patterns of AlOOH adsorbents prepared at different hydrolysis pH values. As AlOOH is an amphoteric oxyhydroxide, it can react with an acid or a base. When the hydrolysis pH value is below 5 or above 10, some AlOOH precipitate will dissolve. Therefore, the hydrolysis pH range was selected from 5 to 10. It can be seen that the phase constituents of AlOOH adsorbents are closely related to the

https://doi.org/10.1021/acsomega.1c01620
ACS Omega 2021, 6, 16488−16497

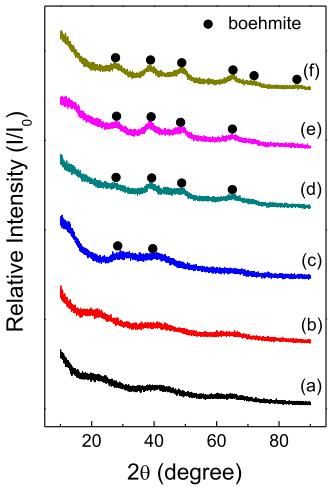

Figure 2. X-ray patterns of (a) AH-5, (b) AH-6, (c) AH-7, (d) AH-8, (e) AH-9, and (f) AH-10 adsorbents.

hydrolysis pH value. The adsorbents transform from amorphous AlOOH to crystalline AlOOH when increasing the hydrolysis pH value. For AlOOH prepared at pH values of 5 and 6, there is almost no diffraction peak, indicating that the adsorbents are amorphous. However, when the hydrolysis pH value is above 6, all available diffraction peaks correspond well with the XRD pattern of boehmite (AlOOH) with the JCPDS No. 21-1307 standard, indicating that the adsorbents are crystalline AlOOH.[33,38] Furthermore, when increasing the hydrolysis pH value from 7, the diffraction peak intensity of AlOOH gradually increases, meaning that increasing the hydrolysis pH value enhances the crystallinity of AlOOH adsorbents.

Figure 3 shows the Fourier transform infrared (FTIR) spectra of AlOOH adsorbents prepared at different hydrolysis

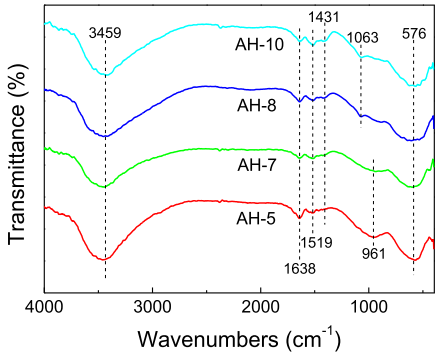

Figure 3. FTIR spectra of AlOOH adsorbents prepared at different hydrolysis pH values.

pH values. All of the AlOOH adsorbents prepared at different hydrolysis pH values have almost the same FTIR spectra. The band of 3459 cm^{-1} represents the physically adsorbed water, and the band of 1638 cm^{-1} results from the bending vibrations of hydroxyl groups originating from adsorbed water.[36,39] The peaks at 1519 and 1431 cm^{-1} are ascribed to the stretching and bending vibrations of Al−O, respectively.[34] The peak at 961 cm^{-1} for AH-5 and AH-7 and the peak at 1063 cm^{-1} for AH-8 and AH-10 correspond to the surface hydroxyl groups.[36] This difference in peak position may be attributed to the phase transformation from amorphous to crystalline AlOOH. In addition, the peak intensity of AH-5 is much stronger than that of the other AlOOH adsorbents, indicating that AH-5 has more surface hydroxyl groups. The band of 576 cm^{-1} belongs to the Al−O−H bending mode.[40]

Figure 4 presents the N_2 adsorption−desorption isotherms and pore size distribution of AlOOH adsorbents prepared at different hydrolysis pH values. Based on the IUPAC classification, the isotherms of AlOOH adsorbents belong to type IV isotherms, which indicate the presence of mesopores (Figure 4a). It is found that the pore size distributions of AH-5, AH-7, and AH-8 have little difference. The pore sizes of AH-5, AH-7, and AH-8 are larger than that of AH-10 (Figure 4b). Table 1 gives the pore volume, average pore size, and BET and external surface area of AlOOH adsorbents prepared at different hydrolysis pH values. It is found that the average pore size of AlOOH adsorbents is 8−13 nm, implying that the pores in AlOOH are mainly mesoporous. The BET surface areas of AH-5, AH-7, AH-8, and AH-10 are 160.3, 139.2, 163.8, and 168.5 m^2/g, respectively. It is interesting that the surface area of AH-7 is the lowest among different AlOOH adsorbents. The point of zero charge (PZC) of AlOOH is 8.5−9.5.[41] When the hydrolysis pH value is below the PZC of AlOOH, the AlOOH adsorbent is protonated and positively charged. In this case, there is an electrostatic repulsion interaction among AlOOH particles, inhibiting the aggregation of AlOOH to a certain extent. For AH-5, it has more surface positive charges than AH-7, making it has more inhibition on aggregation. This explains why the surface area of AH-5 is larger than that of AH-7. As an amorphous material usually has a higher surface energy than a crystalline material,[42] it is more likely to agglomerate. This is the reason why AH-7 has a lower surface area than AH-8 and AH-10.

2.2. Defluoridation Performance of AlOOH Adsorbents. Figure 5 illustrates the fluoride removal efficiency of AlOOH adsorbents prepared at different hydrolysis pH values. Obviously, the hydrolysis pH value has a significant influence on the defluoridation performance of AlOOH adsorbents. AH-5 and AH-6 adsorbents exhibit the best fluoride removal performance, and they can remove >95% fluoride in the first 2 min and reach adsorption equilibrium within 2 h. Furthermore, the residual F^- concentrations for AH-5 and AH-6 are 0.17 and 0.28 mg/L, respectively, which are much lower than the WHO guideline. This means that AH-5 and AH-6 are effective adsorbents for fluoride removal. Increasing the hydrolysis pH value from 6 to 7, the defluoridation performance of AlOOH slightly decreases. However, the defluoridation efficiency decreases dramatically when further increasing the hydrolysis pH value from 7. For the AH-10 adsorbent, the fluoride removal efficiency is only 57.0%. According to the characterization analyses of different AlOOH adsorbents (Figures 1−4 and Table 1), the characterization difference mainly reflects on the crystalline phases of adsorbents (Figure 2). Therefore, it can be inferred that the difference in defluoridation performances of AlOOH adsorbents prepared at different hydrolysis pH values is attributed to the difference in crystalline phases of adsorbents. In addition, it can be concluded that the defluoridation efficiency of amorphous AlOOH is better than that of crystalline AlOOH.

Figure 6 shows the fluoride removal efficiency of AH-5 in an aqueous solution with different initial F^- concentrations. When increasing the initial F^- concentration, the defluoridation efficiency decreases, while the defluoridation capacity increases. The defluoridation efficiency decreases from 99.6

https://doi.org/10.1021/acsomega.1c01620
ACS Omega 2021, 6, 16488−16497

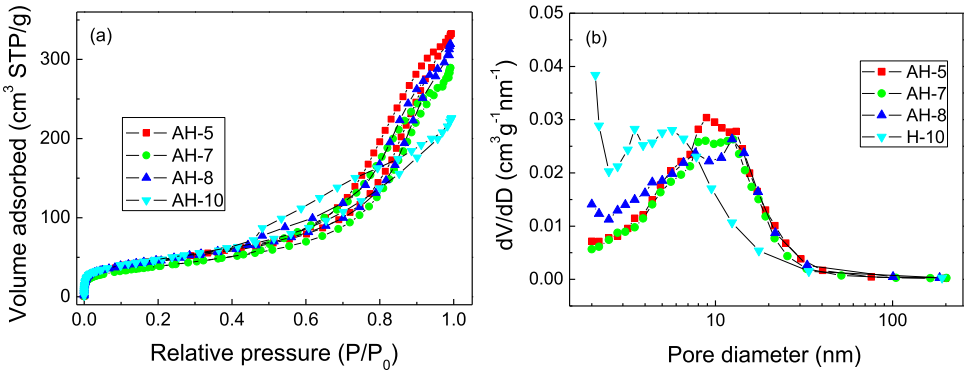

Figure 4. (a) N_2 adsorption−desorption isotherms and (b) pore size distribution of AlOOH adsorbents prepared at different hydrolysis pH values.

Table 1. Pore Volume, Average Pore Size, and BET and External Surface Area of Different AlOOH Adsorbents

adsorbents	average pore size (nm)	pore volume (cm^3/g)	BET surface area (m^2/g)	external surface area (m^2/g)
AH-5	12.8	0.527	160.3	155.3
AH-7	12.9	0.460	139.2	134.4
AH-8	12.1	0.505	163.8	159.2
AH-10	8.3	0.354	168.5	160.7

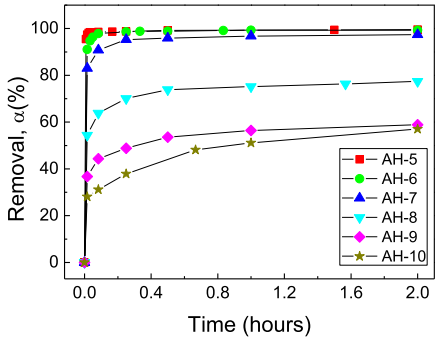

Figure 5. Fluoride removal from the aqueous solution using AlOOH adsorbents prepared at different hydrolysis pH values (C_0 = 40 mg/L, T = 25 °C, adsorbent dose = 2 g/L).

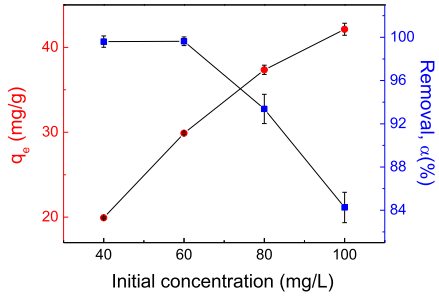

Figure 6. Effect of the initial F^- concentration on fluoride removal from the aqueous solution using the AH-5 adsorbent (T = 25 °C, contact time = 2 h, adsorbent dose = 2 g/L).

to 84.3% when increasing the initial F^- concentration from 40 to 100 mg/L. This is reasonable because the adsorbent cannot provide enough active sites for fluoride adsorption when increasing the initial F^- concentration. For 60 and 80 mg/L F^- solution, the residual F^- concentrations after defluoridation are 0.23 and 5.30 mg/L, respectively. This indicates that AH-5 can effectively remove fluoride from water only when the initial F^- concentration is below 60 mg/L.

As is well known, the pH value of a solution has a great impact on the surface charges of an adsorbent, which in turn affects the defluoridation efficiency of the adsorbent. To research the effect of initial pH value on defluoridation performance, the fluoride removal by AH-5 in a F^- solution with different initial pH values was tested, and the results are shown in Figure 7. Clearly, AH-5 exhibits excellent

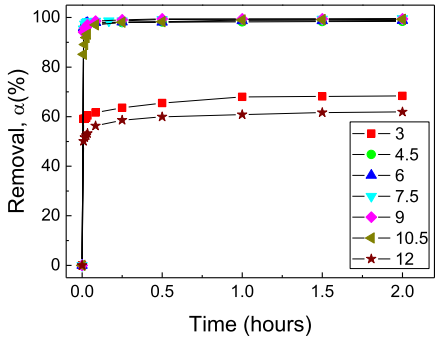

Figure 7. Effect of pH values on fluoride removal from the aqueous solution using the AH-5 adsorbent (C_0 = 40 mg/L, T = 25 °C, adsorbent dose = 2 g/L).

defluoridation efficiency at a wide pH range of 4.5−10.5. When increasing the pH value from 10.5 or decreasing the pH value from 4.5, the defluoridation efficiency decreases drastically. For the F^- solution with pH values of 3 and 12, the defluoridation efficiencies of AH-5 are only 68.3 and 61.9%, respectively. When the pH value is below 4.5, some AH-5 will dissolve, resulting in the decrease of the defluoridation efficiency. When the pH value is above 10.5, AH-5 is deprotonated and there is an electrostatic repulsion between F^- and AH-5, inhibiting the adsorption of fluoride. Moreover, the competition adsorption between F^- and OH^- occurs, which further decreases the defluoridation efficiency.

To investigate the effect of type of Al salts on defluoridation performance, the fluoride removal efficiency of AlOOH adsorbents prepared from $NaAlO_2$, $Al_2(SO_4)_3$, $Al(NO_3)_3$, and $AlCl_3$ at a hydrolysis pH value of 8 was evaluated, as shown in Figure 8. The type of Al salts has little effect on the defluoridation efficiency of AlOOH. In fact, the four types of Al salts are soluble in water, and the anions (AlO_2^-, SO_4^{2-}, NO_3^-, and Cl^-) play no role in the hydrolysis process of Al salts. In addition, the residual anions on the AlOOH surface are removed during the cleaning process. Therefore, the

https://doi.org/10.1021/acsomega.1c01620
ACS Omega 2021, 6, 16488−16497

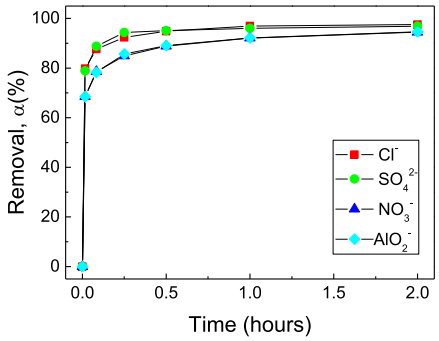

Figure 8. Fluoride removal from the aqueous solution using AlOOH adsorbents prepared from different inorganic Al salts (C_0 = 30 mg/L, T = 25 °C, adsorbent dose = 2 g/L).

AlOOH adsorbents prepared from different Al salts have similar defluoridation performance. However, this result was different from Chai's work, which showed that SO_4^{2-} played a key role in the fluoride removal process.[43] The possible reason is the difference in hydrolysis pH value. In Chai's work, the hydrolysis pH value was 5, which is much lower than PZC. In this case, the adsorbent is protonated and positively charged so that it could attract some SO_4^{2-}. During the defluoridation process, SO_4^{2-} can exchange with F^-.

To further study the defluoridation behavior and determine the adsorption capacity of AlOOH adsorbents, the adsorption isotherm of AH-5 was analyzed. As shown in Figure 9, both the Langmuir and Freundlich isotherm models were used to fit the defluoridation data according to the following equations[44]

$$\text{Langmuir: } \frac{1}{q_e} = \left(\frac{1}{q_{max}K_L}\right)\frac{1}{C_e} + \frac{1}{q_{max}} \quad (1)$$

$$\text{Freundlich: } \log q_e = \log K_F + \frac{1}{n}\log C_e \quad (2)$$

where C_e and q_e are the F^- concentration and the adsorption capacity at equilibrium, respectively; q_{max} is the maximum adsorption capacity; K_L is the binding energy constant; K_F and n are the Freundlich constants corresponding to the adsorption capacity and the favorable degree of adsorption, respectively. Table 2 presents the isotherm model parameters for F^- adsorption by AH-5. According to the correlation coefficient (R^2), adsorption data of AH-5 fit better with the Langmuir model than the Freundlich model, meaning that the adsorption of fluoride on AH-5 is monolayer adsorption. Based on the

Table 2. Isotherm Model Parameters for F^- Adsorption by AH-5

Langmuir			Freundlich		
q_{max} (mg/g)	K_L (L/mg)	R^2	K_F	n	R^2
41.9	5.76	0.920	29.55	7.25	0.758

Langmuir model, the maximum adsorption capacity of AH-5 is 41.9 mg/g, which is consistent with the results of Figure 6 (the adsorption capacity is 42.1 mg/g at the initial F^- concentration of 100 mg/L). This further confirms that the adsorption of fluoride on AH-5 follows the Langmuir model. Adsorption capacities of AlOOH from the present study were compared with those of the other Al-based adsorbents, as shown in Table 3. It can be seen that AlOOH exhibits excellent defluoridation capacity and fast adsorption rate, indicating that AlOOH is a promising defluoridation adsorbent.

To evaluate the reusability of AlOOH adsorbents, AH-5 after defluoridation was regenerated using 1 mol/L NaOH solution, and five successive adsorption−desorption cycles were carried out, as shown in Figure 10. It can be seen that AlOOH can be regenerated using the NaOH solution, and 94.0% fluoride is desorbed from AlOOH in the first cycle. The desorption efficiency decreased with the increase of the cycle number, and only 64.0% fluoride was desorbed after 5 cycles, implying that AlOOH can only be partially regenerated. The fluoride removal efficiency continuously decreased with the cycle number. After five cycles, the fluoride removal efficiency decreased from 93.4 to 56.4%. The decrease of the removal efficiency was caused by the inadequate regeneration of AlOOH.

2.3. Water Quality Assessment after Defluoridation.

The water quality after fluoride removal is an important index to evaluate the defluoridation performance of an adsorbent. As is well known, some aluminum dissolves into water in the defluoridation process using Al-based materials as adsorbents. Al is a potential neurotoxin, and its WHO limit in drinking water is 0.2 mg/L.[29] Long-term drinking water with excessive Al may enhance the risk for the development of Alzheimer's disease in humans.[45] Therefore, it is necessary and meaningful to evaluate the residual Al after defluoridation by AlOOH adsorbents.

Figure 11 demonstrates the residual Al concentration of an aqueous solution after fluoride removal using AlOOH adsorbents prepared at different hydrolysis pH values. As can be seen, the hydrolysis pH value has a great effect on the residual Al. The relationship between residual Al and the

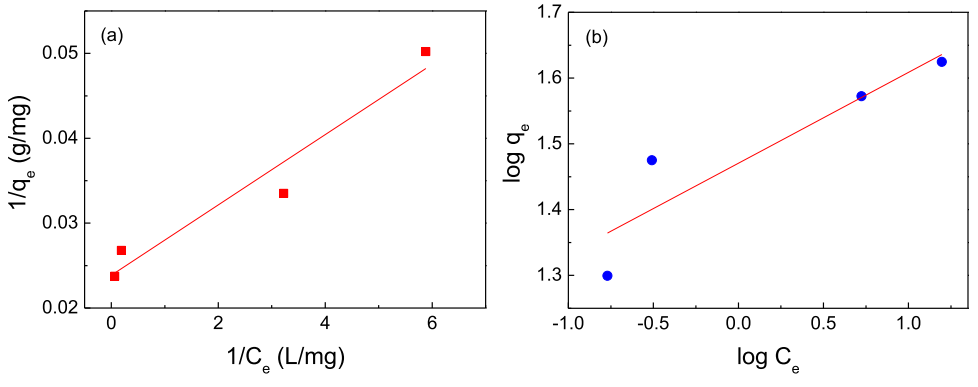

Figure 9. Langmuir (a) and Freundlich (b) adsorption isotherms for fluoride removal from the aqueous solution using the AH-5 adsorbent.

https://doi.org/10.1021/acsomega.1c01620
ACS Omega 2021, 6, 16488−16497

Table 3. Adsorption Capacities of Different Al-Based Adsorbents for Fluoride Removal from Water

adsorbents	C_0 (mg/L)	pH	contact time (h)	q_{max} (mg/g)	refs
Al-modified magnetite ore	1−30	7.8	24	1.51	6
Al/Fe oxide-loaded tea waste	5−200	5.0−10.0	5	18.52	8
Al_2O_3-modified expanded graphite	3−100	4.0	2.5	5.75	10
γ-AlOOH@chitosan shell@Fe_3O_4	5−100	7.0	1	67.5	13
mesoporous $CoAl_2O_4$	5−50	7.0	5	14.80	14
Al_2O_3 nanoparticles	1−50	5−6	6	9.73	24
amorphous Al_2O_3 microsphere	5−150	7.0	10	126.9	26
MgO-loaded Al_2O_3	5−1000	6.8	8	37.35	27
AlOOH@reduced graphene oxide	10−350	6.5	24	118.7	31
bayerite/boehmite	10−100	7.0	5	56.80	36
amorphous AlOOH	30−100	4.5−10.5	2	41.9	this study

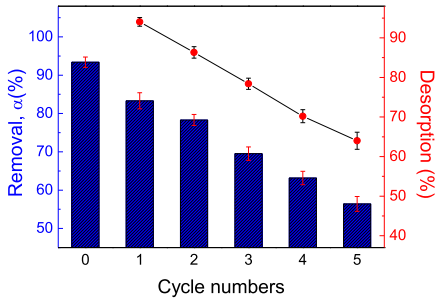

Figure 10. Fluoride adsorption and desorption efficiencies of the AH-5 adsorbent in successive cycles (C_0 = 80 mg/L, T = 25 °C, adsorbent dose = 2 g/L).

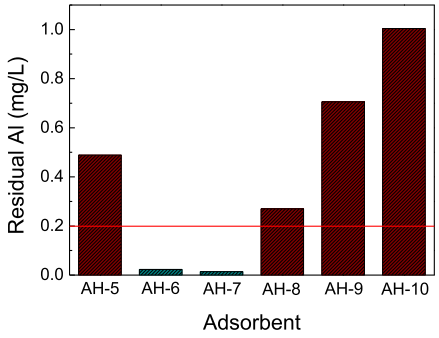

Figure 11. Residual Al concentration of the aqueous solution after fluoride removal using AlOOH adsorbents prepared at different hydrolysis pH values (C_0 = 40 mg/L, T = 25 °C, adsorbent dose = 2 g/L), where the red line refers to the WHO limit of Al in drinking water.

hydrolysis pH value is nonmonotonic, and AlOOH exhibits the lowest residual Al at hydrolysis pH 7. At a hydrolysis pH value of > 7, the amount of HCl is insufficient for the complete hydrolysis of $NaAlO_2$. In this case, some $NaAlO_2$ is not hydrolyzed, and a few AlO_2^- adsorb on the AlOOH surface. Therefore, the residual Al increases with the increase of the hydrolysis pH value when the hydrolysis pH value is above 7. However, at a hydrolysis pH value of < 7, the amount of HCl is excessive for the complete hydrolysis of $NaAlO_2$. In this case, some AlOOH dissolves and releases Al^{3+}, some of which adsorb on the AlOOH surface. Therefore, the residual Al increases with the decrease of the hydrolysis pH value when the hydrolysis pH value is below 7. For AH-6 and AH-7 adsorbents, the residual Al concentrations are 0.023 and 0.014 mg/L, respectively, which are far below the WHO limit. As the defluoridation efficiencies of AH-6 and AH-7 are 99.3 and 97.6% (Figure 5), it can be concluded that the optimum hydrolysis pH value is 6.

2.4. Fluoride Removal Mechanism. It is significant to comprehend the fluoride removal mechanisms, which is helpful to research and improve the defluoridation performances of adsorbents. The fluoride adsorption on AlOOH can be explained using ligand exchange theory. As is well known, there is a layer of hydroxyl groups on the surfaces of AlOOH.[46] To a certain degree, the surface hydroxyl group can be understood as a Lewis base, which has an oxygen atom as a donor that coordinates with Al ions (Lewis acid). The Al ions can exchange the hydroxyl group with other coordinating anions.[47] Moreover, AlOOH has a stronger affinity for fluoride than the hydroxyl group.[48] Therefore, when the AlOOH

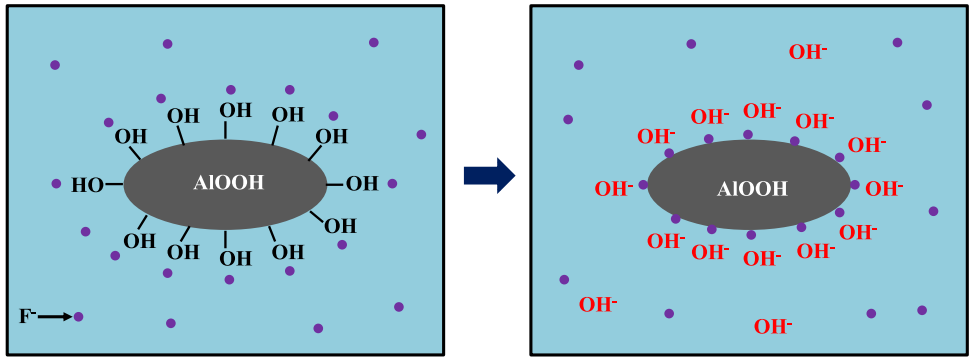

Figure 12. Schematic representation of fluoride removal from the aqueous solution using AlOOH adsorbents.

https://doi.org/10.1021/acsomega.1c01620
ACS Omega 2021, 6, 16488−16497

adsorbents are put into a F^- solution, the hydroxyl groups can exchange with F^-, as shown in Figure 12.

$$F^- + \equiv AlOH \leftrightarrow \equiv AlF + OH^- \quad (3)$$

where ≡ AlOH represents the hydroxyl group on the AlOOH surface. After the reaction, fluoride adsorbs on the adsorbent surface, and OH^- is released into the aqueous solution.

To confirm the above fluoride removal mechanism, FTIR and X-ray photoelectron spectroscopy (XPS) were used to analyze the AlOOH adsorbents before and after fluoride removal. Figure 13 illustrates the FTIR spectra of AH-5 before and after adsorption. It is found that the peak at 961 cm^{-1} corresponding to the surface hydroxyl groups obviously decreases after fluoride adsorption, indicating that surface hydroxyl groups are involved in the fluoride adsorption process. This validates that the exchange between surface hydroxyl groups and fluoride is the main mechanism for fluoride removal.

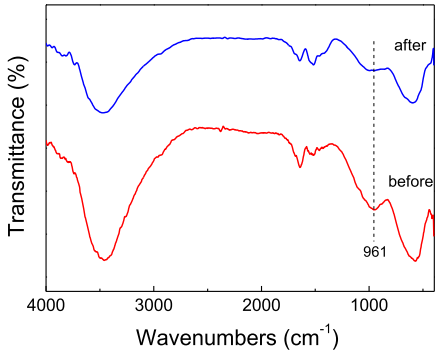

Figure 13. FTIR spectra of the AH-5 adsorbent before and after fluoride removal (C_0 = 100 mg/L, T = 25 °C, adsorbent dose = 2 g/L).

Figure 14 shows the XPS survey spectra and XPS spectra of F 1s, Al 2p and O 1s of the AH-5 adsorbent before and after fluoride removal. As can be seen from Figure 14a, a new peak at 684.9 eV appears after fluoride removal, which corresponds to the F 1s spectrum further confirmed by Figure 14b. Similar results have been obtained in a H_2O_2-modified alumina adsorbent and an oxalic modified Ce−AlOOH adsorbent.[28,33] To further analyze the XPS results, the Al 2p and O 1s spectra are fitted by the Gaussian−Lorentzian function, and the fitting results are given in Figures 14c,d and Table 4. The Al 2p spectrum of AH-5 can be resolved to two peaks located at 74.1 and 74.6 eV, which are assigned to Al−O and Al−OH, respectively.[49] After fluoride removal, in the Al 2p spectrum, three peaks are observed. The new peak at 75.4 eV is assigned to Al−F,[36,50] implying that fluoride adsorbs on AH-5. The content of Al−OH in Al 2p spectra decreases from 84.55 to 64.38% after fluoride removal, indicating that hydroxyl groups are involved in the fluoride removal process. For O 1s spectra (Figure 14d), the peaks at 530.6, 532.0, and 533.0 correspond to Al−O−Al, Al−OH, and H_2O, respectively.[36,51] After fluoride removal, the content of Al−OH decreases from 82.91 to 72.02%, which further confirms that the surface

Table 4. Al 2p and O 1s Peak Parameters for the AH-5 Adsorbent before and after Fluoride Removal

electrons	peak	binding energy (eV)	before adsorption (%)	after adsorption (%)
Al 2p	Al−O	73.9	15.45	22.06
	Al−OH	74.5	84.55	64.38
	Al−F	75.4		13.56
O 1s	Al−O−Al	530.6	9.20	14.56
	Al−OH	532.0	82.91	72.02
	H_2O	533.0	7.89	13.42

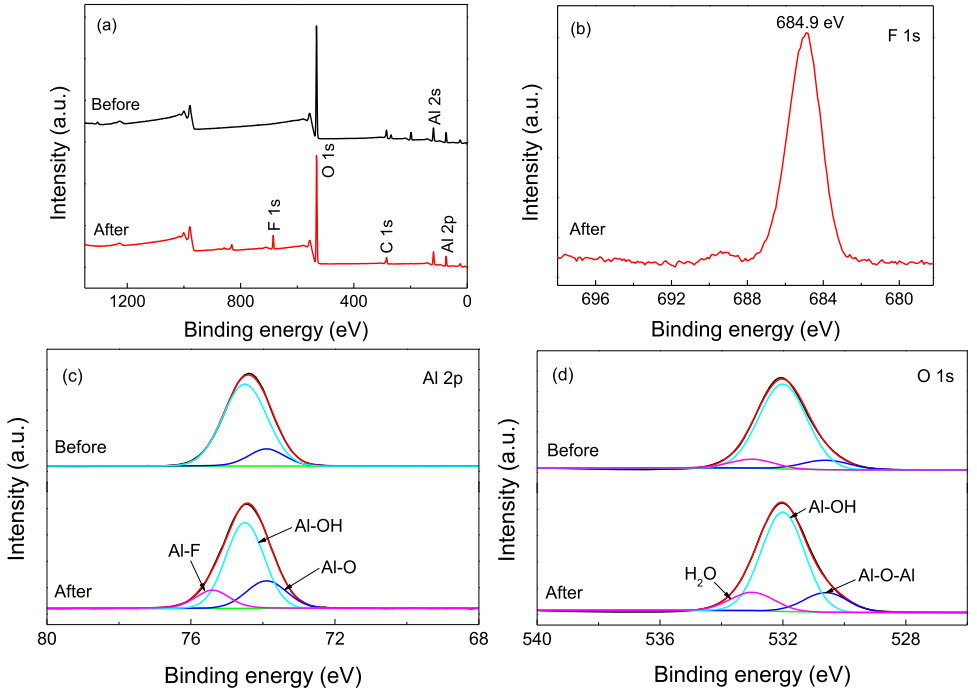

Figure 14. (a) XPS survey spectra and XPS spectra of (b) F 1s, (c) Al 2p, and (d) O 1s of the AH-5 adsorbent before and after fluoride removal (C_0 = 100 mg/L, T = 25 °C, adsorbent dose = 2 g/L).

https://doi.org/10.1021/acsomega.1c01620
ACS Omega 2021, 6, 16488−16497

hydroxyl groups are the active sites for fluoride adsorption. This is in agreement with the results of Al 2p spectra and FTIR spectra. Therefore, it can be concluded that the exchange between fluoride and surface hydroxyl groups is the main fluoride removal mechanism of AlOOH adsorbents.

3. CONCLUSIONS

In this work, amorphous and crystalline AlOOH adsorbents were synthesized through hydrolysis of Al salts, and their feasibility for fluoride removal was evaluated. It is found that the defluoridation performance of AlOOH is closely related to the hydrolysis pH value but hardly to the type of Al salts. AlOOH prepared at a hydrolysis pH value of 5 exhibited the best fluoride removal efficiency. Increasing the hydrolysis pH value from 5 to 10, the adsorbent transforms from amorphous to crystalline AlOOH, and the defluoridation efficiency decreases from 99.6 to 57.0%. AH-5 not only has a fast defluoridation rate but also has a high adsorption capacity. It can remove >95% fluoride in the first 2 min and reach adsorption equilibrium within 2 h, and the maximum defluoridation capacity is 41.9 mg/g. Furthermore, the adsorbent could effectively remove fluoride from water at a wide pH range of 4.5−10.5. After fluoride removal, the adsorbents prepared at pH values of 6 and 7 have low residual Al concentration. The FTIR and XPS results confirm that the fluoride removal mechanism is the ligand exchange between fluoride and hydroxyl groups. Based on the outstanding performance of high adsorption capacity, fast defluoridation rate, and low residual Al concentration, AH-6 is a promising adsorbent for fluoride removal.

4. EXPERIMENTAL PROCEDURE

4.1. Preparation of AlOOH Adsorbents. $NaAlO_2$, $Al_2(SO_4)_3{\cdot}18H_2O$, $Al(NO_3)_3{\cdot}9H_2O$, $AlCl_3$, $NH_3{\cdot}H_2O$, NaOH, HCl, NaF, and absolute ethanol were purchased from Sinopharm Chemical Reagent Co., Ltd. All of the chemical reagents were of analytical reagent grade and were used as received. Amorphous or crystalline AlOOH adsorbents were prepared through hydrolysis of Al salts. First, 1 g of $NaAlO_2$ was dissolved in 100 mL of deionized water, and then diluted HCl solution was added dropwise through a PTFE burette until the pH value of suspension reached the predetermined values (5−10). In this process, a white precipitate was gradually formed

$$NaAlO_2 + HCl \rightarrow AlOOH \downarrow + NaCl \quad (4)$$

Subsequently, the suspension was filtered by vacuum filtration and washed four times with deionized water and once with absolute ethanol. Finally, the obtained precipitate was dried at 60 °C for 10 h and then sieved using a 200 mesh nylon sieve. The AlOOH adsorbent is labeled as AH-N, where "N" represents the hydrolysis pH value.

To study the effect of Al salt type on defluoridation performance of AlOOH, $Al_2(SO_4)_3$, $Al(NO_3)_3$, and $AlCl_3$ were used as Al sources to prepare AlOOH adsorbents, and the preparation procedure was similar to that of using $NaAlO_2$ as the Al source. First, 1 g of Al salt was dissolved in 100 mL of deionized water, and then diluted $NH_3{\cdot}H_2O$ solution was added dropwise until the pH value of suspension reached 8. In this process, a white precipitate was gradually formed

$$Al^{3+} + 3NH_3{\cdot}H_2O \rightarrow AlOOH \downarrow + 3NH_4^+ + H_2O \quad (5)$$

After that, the suspension was filtered, cleaned, dried, and sieved.

4.2. Fluoride Removal Tests. A stock solution with 1000 mg/L F^- was obtained through dissolving an appropriate amount of NaF in deionized water. The aqueous solution with different initial F^- concentrations was prepared by diluting the F^- stock solution with deionized water. In each fluoride removal test, 0.5 g of an AlOOH adsorbent was added into a PTFE beaker containing 250 mL of the F^- solution. To improve the adsorption efficiency, the suspension was stirred at a speed of 500 rpm using a magnetic stirrer. All of the adsorption tests were conducted at 25 ± 1 °C, which was controlled by a thermostatic water bath. At a predetermined time, 10 mL of suspension was collected from the beaker using a syringe-driven filter with a 0.22 μm polyethersulfone (PES) membrane. After the adsorption test, the adsorbent was recovered by filtering and drying and used for further analysis. In the tests of analyzing the effect of pH value on the defluoridation efficiency, the pH value of the F^- solution was adjusted using the NaOH or HCl solution. To ensure the reproducibility, each fluoride removal test was carried out three times and the average values were used.

4.3. Chemical Analyses. The concentration of fluoride in the aqueous solution was measured using an ion meter (PXSJ-216, Inesa Scientific Instrument Co., Shanghai, China) with a fluoride ion-selective electrode. The fluoride removal efficiency α can be obtained using the following equation

$$\alpha = \frac{C_0 - C_t}{C_0} \quad (6)$$

where C_0 is the initial F^- concentration and C_t is the F^- concentration in the aqueous solution at time t.

The pH value of the F^- solution before and after fluoride removal was determined using a pH meter (PHS-3E, Inesa Scientific Instrument Co., Shanghai, China). The crystalline phases and morphology of adsorbents were analyzed using X-ray diffractometry (XRD, D8 Advance, Germany) and scanning electron microscopy (SEM, Sigma 500/VP, Germany), respectively. The specific surface area and pore characteristics of adsorbents were examined using a surface area analyzer (ASAP 2020). The functional groups and chemical bonds of adsorbents before and after fluoride removal were analyzed using a Fourier transform infrared spectrometer (FTIR, Avatar 370). The surface element chemical states of adsorbents before and after fluoride removal were acquired by X-ray photoelectron spectroscopy (XPS, ESCALAB250Xi). An inductively coupled plasma atomic emission spectrometer (ICP-AES, ICAP 6300) was used to analyze the residual Al concentration in solution after defluoridation.

AUTHOR INFORMATION

Corresponding Author

Wei-Zhuo Gai − *College of Physics and Electronic Information & Henan Key Laboratory of Electromagnetic Transformation and Detection, Luoyang Normal University, Luoyang 471934, China;* orcid.org/0000-0001-8815-1919; Email: gaiweizhuo@126.com

Authors

Shi-Hu Zhang − *College of Physics and Electronic Information & Henan Key Laboratory of Electromagnetic Transformation and Detection, Luoyang Normal University, Luoyang 471934, China*

https://doi.org/10.1021/acsomega.1c01620
ACS Omega 2021, 6, 16488−16497

Yang Yang − *Energy Materials & Physics Group, Department of Physics, Shanghai University, Shanghai 200444, China*
Xianghui Zhang − *College of Physics and Electronic Information & Henan Key Laboratory of Electromagnetic Transformation and Detection, Luoyang Normal University, Luoyang 471934, China;* orcid.org/0000-0002-6709-6073
Zhen-Yan Deng − *Energy Materials & Physics Group, Department of Physics, Shanghai University, Shanghai 200444, China;* orcid.org/0000-0002-4368-7039

Complete contact information is available at: https://pubs.acs.org/10.1021/acsomega.1c01620

Notes

The authors declare no competing financial interest.

■ ACKNOWLEDGMENTS

This work was supported by the National Natural Science Foundation of China (Grant no. 51872181).

■ REFERENCES

(1) Gai, W.-Z.; Deng, Z. Y.; Shi, Y. Fluoride removal from water using High-activity aluminum hydroxide prepared by the ultrasonic method. *RSC Adv.* **2015**, *5*, 84223−84231.
(2) Vinati, A.; Mahanty, B.; Behera, S. K. Clay and clay minerals for fluoride removal from water: a state-of-the-art review. *Appl. Clay Sci.* **2015**, *114*, 340−348.
(3) Khandare, D.; Mukherjee, S. A review of metal oxide nanomaterials for fluoride decontamination from water environment. *Mater. Today: Proc.* **2019**, *18*, 1146−1155.
(4) Alkurdi, S. S. A.; Al-Juboori, R. A.; Bundschuh, J.; Hamawand, I. Bone char as a green sorbent for removing health threatening fluoride from drinking water. *Environ. Int.* **2019**, *127*, 704−719.
(5) Bhatnagar, A.; Kumar, E.; Sillanpää, M. Fluoride removal from water by adsorption-a review. *Chem. Eng. J.* **2011**, *171*, 811−840.
(6) García-Sánchez, J. J.; Solache-Ríos, M.; Martínez-Gutiérrez, J. M.; Arteaga-Larios, N. V.; Ojeda-Escamilla, M. C.; Rodríguez-Torres, I. Modified natural magnetite with Al and La ions for the adsorption of fluoride ions from aqueous solutions. *J. Fluorine Chem.* **2016**, *186*, 115−124.
(7) Sepehr, M. N.; Sivasankar, V.; Zarrabi, M.; Kumar, M. S. Surface modification of pumice enhancing its fluoride adsorption capacity: an insight into kinetic and thermodynamic studies. *Chem. Eng. J.* **2013**, *228*, 192−204.
(8) Cai, H.-m.; Chen, G. J.; Peng, C. Y.; Zhang, Z. Z.; Dong, Y. Y.; Shang, G. Z.; Zhu, X. H.; Gao, H. J.; Wan, X. C. Removal of fluoride from drinking water using tea waste loaded with Al/Fe oxides: a novel, safe and efficient biosorbent. *Appl. Surf. Sci.* **2015**, *328*, 34−44.
(9) Zúñiga-Muro, N. M.; Petriciolet, A. B.; Castillo, D. I. M.; Avila, H. E. R.; Picazo, J. C. T. Fluoride adsorption properties of cerium-containing bone char. *J. Fluorine Chem.* **2017**, *197*, 63−73.
(10) Jin, H.; Ji, Z. J.; Yuan, J.; Li, J.; Liu, M.; Xu, C. H.; Dong, J.; Hou, P.; Hou, S. Research on removal of fluoride in aqueous solution by alumina-modified expanded graphite composite. *J. Alloys Compd.* **2015**, *620*, 361−367.
(11) Mei, L.; Qiao, H. H.; Ke, F.; Peng, C. Y.; Hou, R. Y.; Wan, X. C.; Cai, H. M. One-step synthesis of zirconium dioxide-biochar derived from Camellia oleifera seed shell with enhanced removal capacity for fluoride from water. *Appl. Surf. Sci.* **2020**, *509*, No. 144685.
(12) Takmil, F.; Esmaeili, H.; Mousavi, S. M.; Hashemi, S. A. Nano-magnetically modified activated carbon prepared by oak shell for treatment of wastewater containing fluoride ion. *Adv. Powder Technol.* **2020**, *31*, 3236−3245.
(13) Wan, Z.; Chen, W.; Liu, C.; Liu, Y.; Dong, C. L. Preparation and characterization of γ-AlOOH @CS magnetic nanoparticle as a novel adsorbent for removing fluoride from drinking water. *J. Colloid Interface Sci.* **2015**, *443*, 115−124.
(14) Zhao, X.; Zhang, L. M.; Xiong, P.; Ma, W. J.; Qian, N.; Lu, W. C. A novel method for synthesis of Co-Al layered double hydroxides and their conversions to mesoporous $CoAl_2O_4$ nanostructures for applications in adsorption removal of fluoride ions. *Microporous Mesoporous Mater.* **2015**, *201*, 91−98.
(15) Vences-Alvarez, E.; Arciniega, J. L. F.; Zuñiga, H. F.; Mendez, J. R. R. Fluoride removal from water by ceramic oxides from cerium and manganese solutions. *J. Mol. Liq.* **2019**, *286*, No. 110880.
(16) Pillai, P.; Lakhtaria, Y.; Dharaskar, S.; Khalid, M. Synthesis, characterization, and application of iron oxyhydroxide coated with rice husk for fluoride removal from aqueous media. *Environ. Sci. Pollut. Res.* **2020**, *27*, 20606−20620.
(17) Sani, T.; Gómez-Hortigüela, L.; Pérez-Pariente, J.; Chebude, Y.; Díaz, I. Defluoridation performance of nano-hydroxyapatite/stilbite composite compared with bone char. *Sep. Purif. Technol.* **2016**, *157*, 241−248.
(18) Affonso, L. N., Jr.; J, L. M.; Lima, V. V. C.; Goncalves, J. O.; Barbosa, S. C.; Primel, E. G.; Burgo, T. A. L.; Dotto, G. L.; Pinto, L. A. A., Jr.; T, R. S. G. Removal of fluoride from fertilizer industry effluent using carbon nanotubes stabilized in chitosan sponge. *J. Hazard. Mater.* **2020**, *388*, No. 122042.
(19) Chen, P.; Wang, T.; Xiao, Y. W.; Tian, E. X.; Wang, W. L.; Zhao, Y. L.; Tian, L.; Jiang, H. L.; Luo, X. B. Efficient fluoride removal from aqueous solution by synthetic Fe-Mg-La tri-metal nano-composite and the analysis of its adsorption mechanism. *J. Alloys Compd.* **2018**, *738*, 118−129.
(20) He, J.; Zhang, K. S.; Wu, S. B.; Cai, X. G.; Chen, K.; Li, Y. L.; Sun, B.; Jia, Y.; Meng, F. L.; Jin, Z.; Kong, L. T.; Liu, J. H. Performance of novel hydroxyapatite nanowires in treatment of fluoride contaminated water. *J. Hazard. Mater.* **2016**, *303*, 119−130.
(21) Ghorai, S.; Pant, K. K. Investigations on the column performance of fluoride adsorption by activated alumina in a fixed-bed. *Chem. Eng. J.* **2004**, *98*, 165−173.
(22) Tang, Y.; Guan, X. H.; Su, T. Z.; Gao, N. Y.; Wang, J. M. Fluoride adsorption onto activated alumina: modeling the effects of pH and some competing ions. *Colloids Surf., A* **2009**, *337*, 33−38.
(23) Camacho, L. M.; Torres, A.; Saha, D.; Deng, S. G. Adsorption equilibrium and kinetics of fluoride on sol−gel-derived activated alumina adsorbents. *J. Colloid Interface Sci.* **2010**, *349*, 307−313.
(24) Tangsir, S.; Hafshejani, L. D.; Lähde, A.; Maljanen, M.; Hooshmand, A.; Naseri, A. A.; Moazed, H.; Jokiniemi, J.; Bhatnagar, A. Water defluoridation using Al_2O_3 nanoparticles synthesized by flame spray pyrolysis (FSP) method. *Chem. Eng. J.* **2016**, *288*, 198−206.
(25) Yang, C.; Gao, L. L.; Wang, Y. X.; Tian, X. K.; Komarneni, S. Fluoride removal by ordered and disordered mesoporous aluminas. *Microporous Mesoporous Mater.* **2014**, *197*, 156−163.
(26) Kang, D.; Tong, S. R.; Yu, X. L.; Ge, M. F. Template-free synthesis of 3D hierarchical amorphous aluminum oxide microspheres with broccoli-like structure and their application in fluoride removal. *RSC Adv.* **2015**, *5*, 19159−19165.
(27) Dayananda, D.; Sarva, V. R.; Prasad, S. V.; Arunachalam, J.; Parameswaran, P.; Ghosh, N. N. Synthesis of MgO nanoparticle loaded mesoporous Al_2O_3 and its defluoridation study. *Appl. Surf. Sci.* **2015**, *329*, 1−10.
(28) Huang, L.; Yang, Z. H.; Zhang, Z. X.; Jin, L. F.; Yang, W. C.; He, Y. J.; Ren, L. L.; Wang, H. Y. Enhanced surface hydroxyl groups by using hydrogen peroxide on hollow tubular alumina for removing fluoride. *Microporous Mesoporous Mater.* **2020**, *297*, No. 110051.
(29) George, S.; Pandit, P.; Gupta, A. B. Residual aluminum in water defluoridated using activated alumina adsorption - modeling and simulation studies. *Water Res.* **2010**, *44*, 3055−3064.
(30) Zhao, X.; Wang, J. M.; Wu, F. C.; Wang, T.; Cai, Y. Q.; Shi, Y. L.; Jiang, G. B. Removal of fluoride from aqueous media by Fe_3O_4@$Al(OH)_3$ magnetic nanoparticles. *J. Hazard. Mater.* **2010**, *173*, 102−109.

(31) Sun, R.; Zhang, H. B.; Qu, J.; Yao, H.; Yao, J.; Yu, Z. Z. Supercritical carbon dioxide fluid assisted synthesis of hierarchical AlOOH@reduced graphene oxide hybrids for efficient removal of fluoride ions. *Chem. Eng. J.* **2016**, *292*, 174−182.
(32) Wu, S.; Zhang, K. S.; He, J. Y.; Cai, X. G.; Chen, K.; Li, U. L.; Sun, B.; Kong, L. T.; Liu, J. H. High efficient removal of fluoride from aqueous solution by a novel hydroxyl aluminum oxalate adsorbent. *J. Colloid Interface Sci.* **2016**, *464*, 238−245.
(33) Tao, W.; Zhong, H.; Pan, X. B.; Wang, P.; Wang, H. Y.; Huang, L. Removal of fluoride from wastewater solution using Ce-AlOOH with oxalic acid as modification. *J. Hazard. Mater.* **2020**, *384*, No. 121373.
(34) Liu, R.; Gong, W. X.; Lan, H. C.; Gao, Y. P.; Liu, H. J.; Qu, J. H. Defluoridation by freshly prepared aluminum hydroxides. *Chem. Eng. J.* **2011**, *175*, 144−149.
(35) Du, J.; Sabatini, D. A.; Butler, E. C. Synthesis, characterization, and evaluation of simple aluminum-based adsorbents for fluoride removal from drinking water. *Chemosphere* **2014**, *101*, 21−27.
(36) Jia, Y.; Zhu, B. S.; Jin, Z.; Sun, B.; Luo, T.; Yu, X. Y.; Kong, L. T.; Liu, J. H. Fluoride removal mechanism of bayerite/boehmite nanocomposites: roles of the surface hydroxyl groups and the nitrate anions. *J. Colloid Interface Sci.* **2015**, *440*, 60−67.
(37) Gai, W.-Z.; Zhang, X. H.; Yang, Y.; Deng, Z. Y. Effect of crystalline phases of aluminum hydroxide catalysts on Al-water reaction. *Int. J. Energy Res.* **2020**, *44*, 4969−4976.
(38) Esmaeili, H.; Tamjidi, S. Ultrasonic-assisted synthesis of natural clay/Fe3O4/graphene oxide for enhance removal of Cr (VI) from aqueous media. *Environ. Sci. Pollut. Res.* **2020**, *27*, 31652−31664.
(39) Wang, F.; Wang, K. T.; Muhammad, Y.; Wei, Y. Z.; Shao, L.; Wang, X. P. Preparation of CeO_2@SiO_2 microspheres by a non-sintering strategy for highly selective and continuous adsorption of fluoride ions from wastewater. *ACS Sustainable Chem. Eng.* **2019**, *7*, 14716−14726.
(40) Wang, X.; Andrews, L. Infrared spectroscopic observation of the group 13 metal hydroxides, $M(OH)_{1,2,3}$ (M = Al, Ga, In, and Ti) and $Hal(OH)_2$. *J. Phys. Chem. A* **2007**, *111*, 1860−1868.
(41) Kosmulski, M. Compilation of PZC and IEP of sparingly soluble metal oxides and hydroxides from literature. *Adv. Colloid Interface Sci.* **2009**, *152*, 14−25.
(42) Newell, H. E.; Buckton, G.; Butler, D. A.; Thielmann, F.; Williams, D. R. The use of inverse phase gas chromatography to measure the surface energy of crystalline, amorphous, and recently milled lactose. *Pharm. Res.* **2001**, *18*, 662−666.
(43) Chai, L.; Wang, Y. Y.; Zhao, N.; Yang, W. C.; You, X. Y. Sulfate-doped Fe_3O_4/Al_2O_3 nanoparticles as a novel adsorbent for fluoride removal from drinking water. *Water Res.* **2013**, *47*, 4040−4049.
(44) Srivastav, A. L.; Singh, P. K.; Srivastava, V.; Sharma, Y. C. Application of a new adsorbent for fluoride removal from aqueous solutions. *J. Hazard. Mater.* **2013**, *263*, 342−352.
(45) Rondeau, V.; Commenges, D.; Gadda, H. J.; Dartigues, J. F. Relation between aluminum concentrations in drinking water and Alzheimer's disease: an 8-year follow-up study. *Am. J. Epidemiol.* **2000**, *152*, 59−66.
(46) Sposito, G. *Environmental Chemistry of Aluminum*; CRC Press: California, 1996.
(47) Kummert, R.; Stumm, W. The surface complexation of organic acids on hydrous γ-Al_2O_3. *J. Colloid Interface Sci.* **1980**, *75*, 373−385.
(48) Pommerenk, P.; Schafran, G. C. Adsorption of inorganic and organic ligands onto hydrous aluminum oxide: evaluation of surface charge and the impacts on particle and NOM removal during water treatment. *Environ. Sci. Technol.* **2005**, *39*, 6429−6434.
(49) Iatsunskyi, I.; Kempiński, M.; Jancelewicz, M.; Załęski, K.; Jurga, S.; Smyntyna, V. Structural and XPS characterization of ALD Al_2O_3 coated porous silicon. *Vacuum* **2015**, *113*, 52−58.
(50) Jia, Y.; Zhu, B. S.; Zhang, K. S.; Jin, Z.; Sun, B.; Luo, T.; Yu, X. Y.; Kong, L. T.; Liu, J. H. Porous 2-line ferrihydrite/Bayerite composites (LFBC): fluoride removal performance and mechanism. *Chem. Eng. J.* **2015**, *268*, 325−336.
(51) Zhang, H.; Li, P.; Cui, W. W.; Liu, C.; Wang, S. L.; Zheng, S. L.; Zhang, Y. Synthesis of nanostructured γ-AlOOH and its accelerating behavior on the thermal decomposition of AP. *RSC Adv.* **2016**, *6*, 27235.

https://doi.org/10.1021/acsomega.1c01620
ACS Omega 2021, 6, 16488−16497